Supplementary Materials

A Multifunctional Stimuli-Responsive AIE-Active Schiff Base for Solvatochromism, Mechanochromism, Acidochromism, Cu^{2+} Sensing and DNA Binding

Pankaj Haloi [a], *Ram Kumar Mandal*[a], *Sanchita Das*[b], *Rupam Dinda*[b], *Pranjit Barman*[a]*

[a]Department of Chemistry, National Institute of Technology, Silchar, Assam 788010, India.

[b]Department of Chemistry, National Institute of Technology, Rourkela, Odisha 769008, India.

***Author for correspondence:** Pranjit Barman

(**Email:** *barmanpranjit@yahoo.co.in*)

Table of Contents

List of Figures

1. Experimental Section

1.1 Reagents and Chemicals

The solvents employed in the spectral experiments were obtained from Sigma-Aldrich and were of spectrophotometric grade. The other chemicals used in this research were sourced from commercial suppliers and were used without further purification.

1.2 Instrumentation

The IR spectral data was recorded by Perkin Elmer MIR/FIR-FT-IR spectrophotometer. ^{1}H and ^{13}C nuclear magnetic resonance spectra were recorded using a JEOL JNM ECS400 NMR spectrometer in $CDCl_3$ solvent at 400 MH_z. The chemical shift (δ) values were reported in ppm using TMS as reference standard. The ESI positive mass spectra was taken from XEVOG2-XS QTOF spectrometer in DMSO solvent. UV-visible absorption spectra were obtained by using a Cary 60 absorption spectrophotometer. A HITACHI-F4600 spectrophotometer was utilized to record the fluorescence emission spectra.

1.3 Characterization

Yield: 86%; Pale yellow crystalline solid; melting point: 163-165°*C.*

FTIR (v, cm^{-1}): 3438 (O-H); 2846-2948 (aromatic C-H); 1635 (C=N); 1446 (Aromatic C=C); 1121 (C-O) (**Fig. S1**).

^{1}H NMR (400 MHz, $CDCl_3$) (ppm): δ 12.31 (s, 1H), 8.85 (s, 1H), 7.97 (s, 1H), 7.80 (d, J = 7.1 Hz, 2H), 7.66 (s, 1H), 7.56 (d, J = 3.3 Hz, 2H), 7.45-7.33 (t, J = 7.5 Hz, 5H), 3.35 (t, J = 1.6 Hz, 3H) (**Fig. S2**).

^{13}C NMR (126 MHz, DMSO-D_6) (ppm): δ 163.45, 161.11, 160.62, 158.72, 135.91, 135.16, 132.82, 131.31, 129.53, 128.78, 128.40, 124.51, 119.31, 118.20, 83.46 (**Fig. S3**).

ESI-Mass: Base peak was obtained at m/z = 329.05 $[(C_{16}H_{16}N_2O_2) + H]^+$ = 329.12] which confirmed the formation of the **HL** (**Fig. S4**).

1.4 Preparation of Stock Solutions

~1 mmol stock solutions of **HL** was prepared in four solvents having different polarity. For absorbance and emission analysis, the stock solutions of **HL** was diluted to a concentration of about ~50 μM in a suitable solvent. A combination of ~50 μM THF-water solution was prepared for aggregation investigations. To conduct pH tests, a 1 mmol stock solution was diluted to form a ~50 μM concentration in 1:9 THF-aqueous buffer solution. The pH solution was made by the combination of Na_2HPO_4 and NaH_2PO_4 produced a 0.1 M phosphate buffer. The metal ion solutions of about ~10 mmol were developed in the water medium. Finally, the absorbance and emission spectra were captured after 10 minutes of mixing [1].

1.5 Preparation of Biological Samples

Fresh urine samples were acquired from a participant to investigate the biological samples. Approximately ~10 mL of each sample was combined with ~10 mL of methanol to eliminate proteins. The resultant solutions were centrifuged at 10,000 rpm for ten minutes. The excess fluid was quickly separated and filtered for additional investigation.

1.6 Theoretical Calculations

The quantum chemical investigations were conducted using the GAUSSIAN 16 software [2]. The B3LYP 6-311g+(d, p) basis set was utilized for carrying out the optimization of the ground state configuration of **HL** [3]**.** But, for optimizing the ground state of the complexes of **HL,** the LanL2DZ basic set was selected [4].

1.7 Calculation of Quantum Yield

The fluorescence quantum yield was determined by utilizing Rhodamine B as the standard fluorophore [5].

$$\phi_u = \left(\frac{A_s F_u n_u^2}{A_u F_s n_s^2} \right) \phi_s$$

Where 'ϕ_u' is the quantum yield value of the unidentified fluorophore, 'ϕ_s' is the quantum yield value of the fluorophore taken as the standard reference (ϕ_s = 0.68 in ethanol medium). 'A_u' and 'A_s' are the absorbance values at the excitation wavelength for the unknown and the standard fluorophore, respectively. 'F_u' and 'F_s' are the integrated area of fluorescence intensity for the

unknown and the standard fluorophore, respectively. 'n_u' and 'n_s' are the refractive index of the unknown and the standard fluorophore, respectively [6].

1.8 Determination of Limit of Detection (LOD)

The following equation was used to determine the LOD with the help of fluorescence titration,

$$LOD = 3\sigma/S$$

where σ stands for standard deviation value of blank measurements, and the S denotes slope of the calibration plot of I_0-I vs Cu^{2+} ion concentration, where I_0 & I were emission intensity of ligand in absence and presence of Cu^{2+} ions respectively.

1.9 Determination of Stern-Volmer constant (K_{sv})

The Stern-Volmer formula has been implemented to estimate the degree of fluorescence quenching caused by adding copper ions.

$$\frac{I_o}{I} = 1 + K_{SV} \times [Cu^{2+}]$$

Where, 'K_{sv}' is the Stern-Volmer constant, 'I_o' denotes the intensities of fluorescence in the absence of Cu^{2+} ions at different concentrations and 'I' represents intensities of fluorescence presence of Cu^{2+} ions at different concentrations [7].

1.10 Determination of Binding Constant (K_b)

Based on fluorometric titration data, binding constant (K_b) was determined by Benesi-Hildebrand equation,

$$\frac{1}{I - Io} = \left[\frac{1}{Imax - Io}\right]\left[\frac{1}{Kb.C} + 1\right]$$

where I_o denotes emission intensity of **HL** alone, I denote emission intensity of sensor **HL** in different equivalents of Cu^{2+} ions, I_{max} is emission intensity of senor **HL** when 2 equivalents of Cu^{2+} ions was added and C is copper ion concentration [8].

1.11 DNA Binding Study

1.11.1 By UV-vis Spectroscopy

The DNA binding affinity of **HL** with CT-DNA was examined using UV-vis absorption spectroscopy. The experiment was conducted using a solution of 5 mM tris-HCl buffer at pH 7.4. All DNA solutions were prepared fresh in the buffer immediately before use. The concentration of CT-DNA was evaluated at 260 nm, based on its extinction coefficient (6600 M^{-1} cm^{-1}). Moreover, solution of **HL** (25 μM) were prepared in dimethyl sulfoxide/tris-buffer solution. The **HL** maintained at a constant concentration, were titrated with different concentrations of CT-DNA starting from 0 to 180 μM. The compound-DNA mixtures were allowed to incubate for 5 minutes before UV-visible measurements. Titrations continued until successive additions of CT-DNA no longer caused significant changes in the absorption spectra. The binding association constant (K_b) value of interaction between the complexes and CT-DNA was determined by using the following equation.

$$[DNA]/ (\varepsilon_a - \varepsilon_f) = [DNA]/ (\varepsilon_b - \varepsilon_f) + 1/K_b (\varepsilon_b - \varepsilon_f)$$

where [DNA] represents the concentration of DNA, ε_a is apparent molar extinction coefficient at a specific DNA concentration, ε_f denotes molar extinction coefficient of complexes without DNA, and ε_b corresponds to molar extinction coefficient of complexes in its fully DNA-bound state [9,10].

1.11.2 By Fluorescence spectroscopy

Fluorescence spectrometer was utilized to conduct ethidium bromide (EtBr) displacement assays to evaluate whether the test compounds could replace EtBr in the CT-DNA associated complex. To generate the DNA-EtBr complex, CT-DNA and EtBr were mixed in a 10:1 ratio, and the resulting adduct was excited at 515 nm. Emission spectra were examined in the 500-700 nm range before introducing the test compounds. Fluorescence quenching was observed as a result of the displacement of EtBr, showing that the **HL** competitively bound to DNA. As the concentration of the **HL** increased, changes in the fluorescence intensity of the EtBr-bind CT-DNA complex were monitored [10].

1.12 Molecular Docking Analysis

We carried out a molecular docking study on the proposed ligand using AutoDock 4.2 [11]. The receptor structure was retrieved from the Protein Data Bank. This study investigated the interactions of **HL** with CT-DNA. The ligand structure was geometry optimized using the Gaussian 16 software package, and the molecular docking interactions were analyzed with Biovia Discovery Studio Visualizer 4.0 [12].

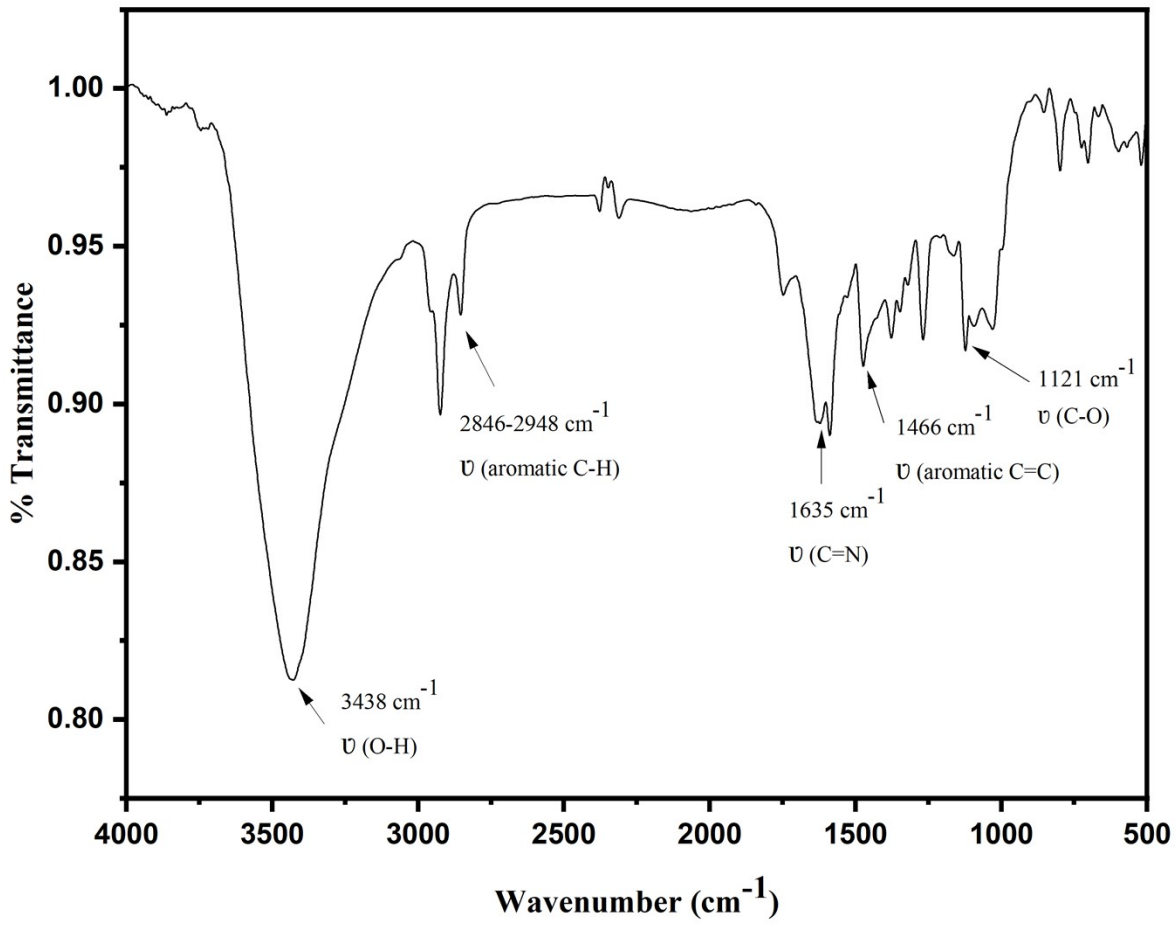

Fig. S1. FT-IR spectra of **HL**

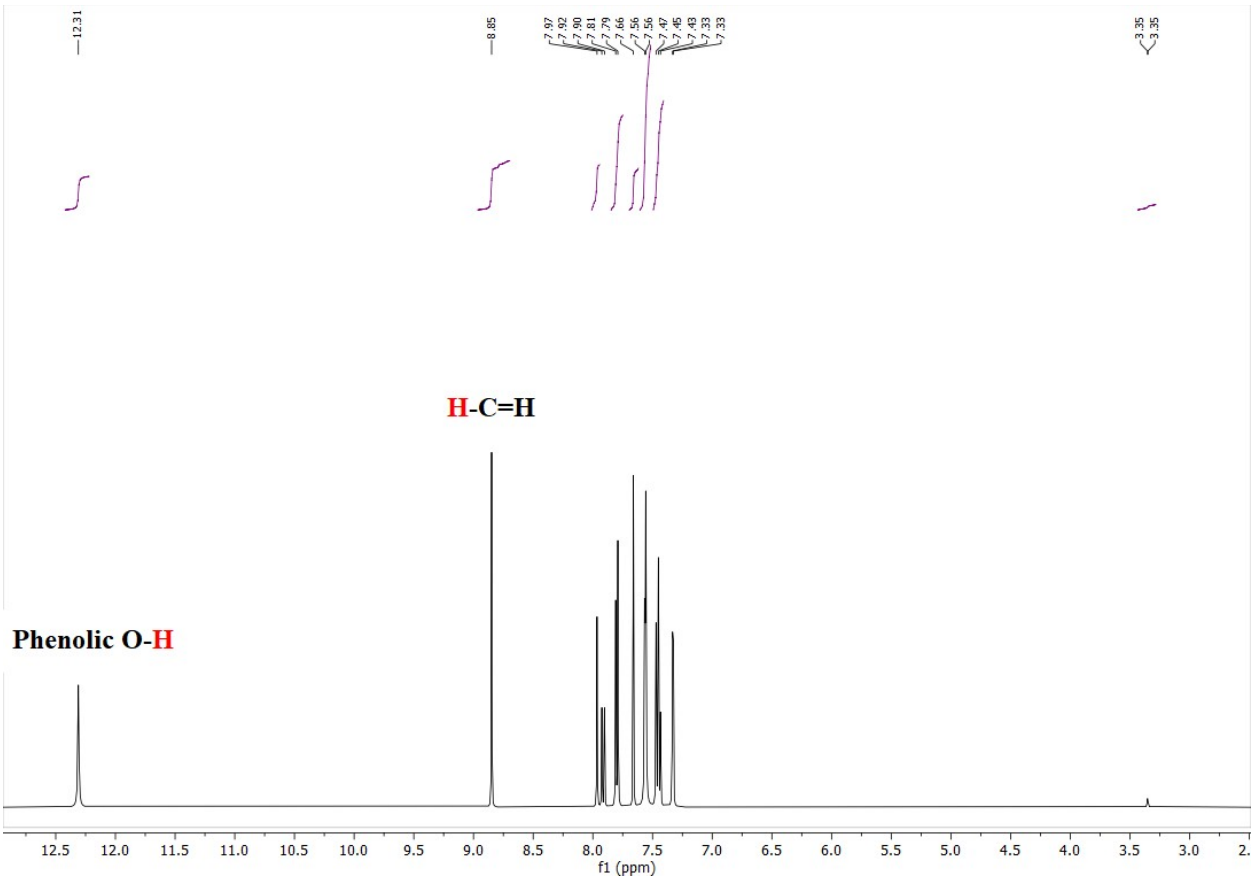

Fig. S2. ^{1}H-NMR spectra of **HL**

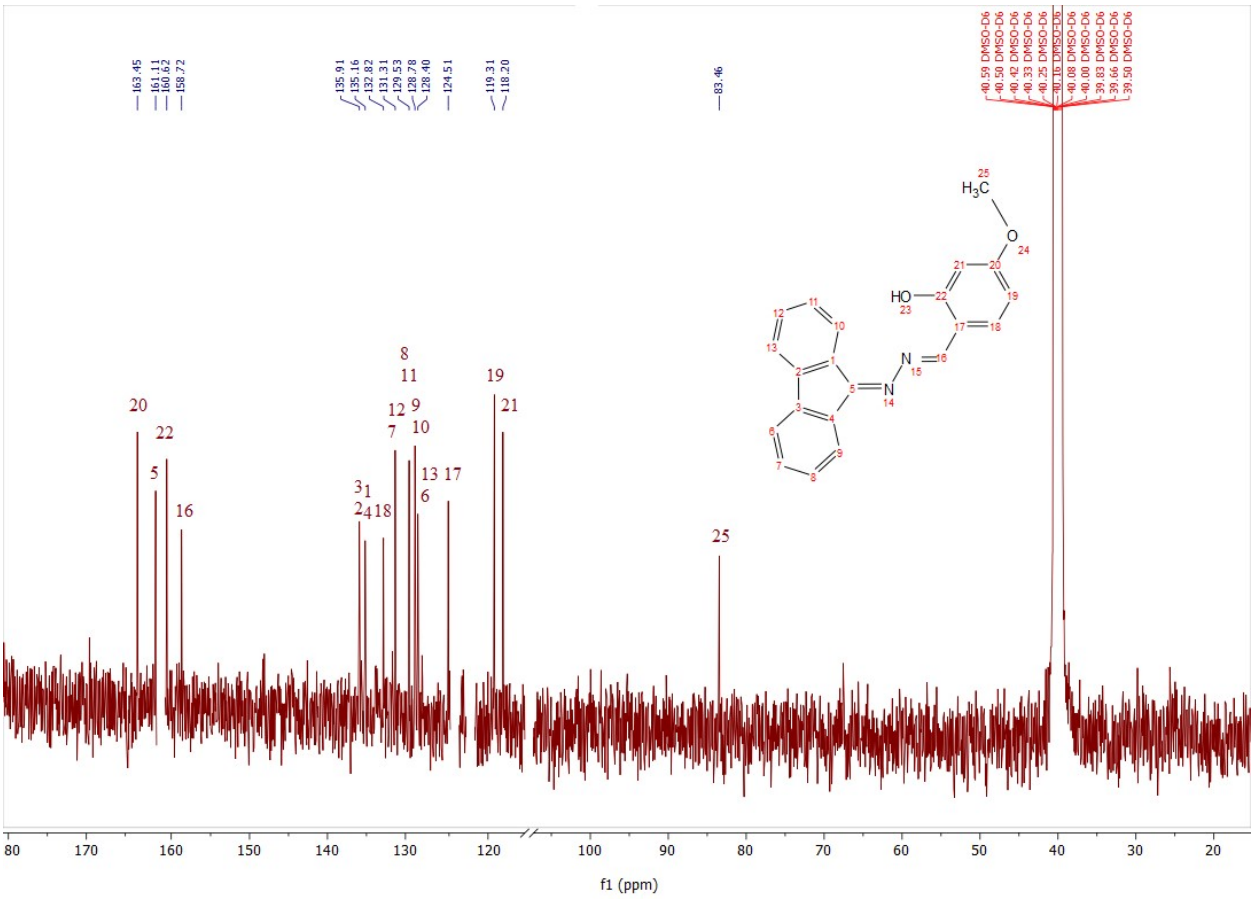

Fig. S3. ^{13}C-NMR spectra of **HL**

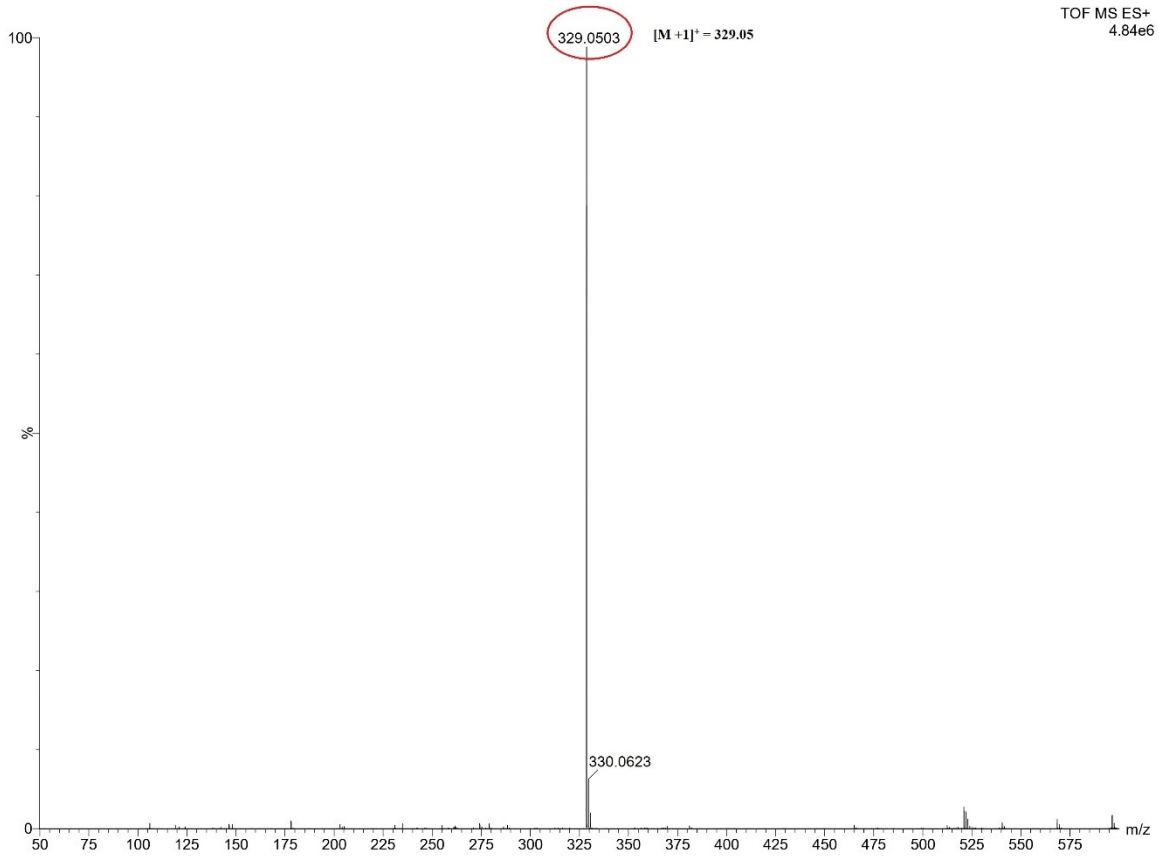

Fig. S4. ESI-MS spectra of **HL**

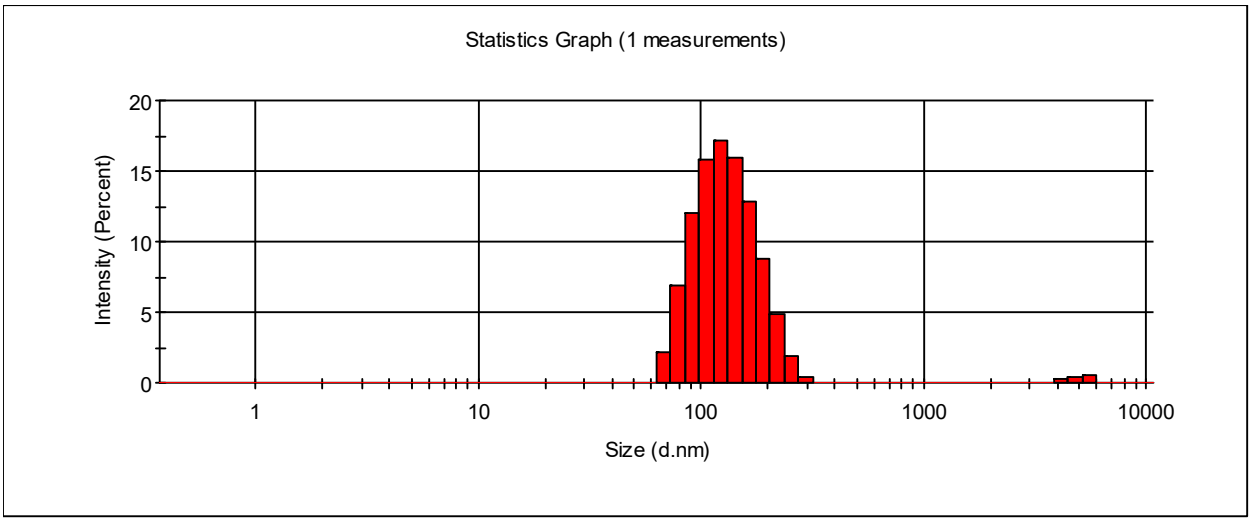

Fig. S5 (a). DLS data of **HL** (25 μM) at f_w = 30%

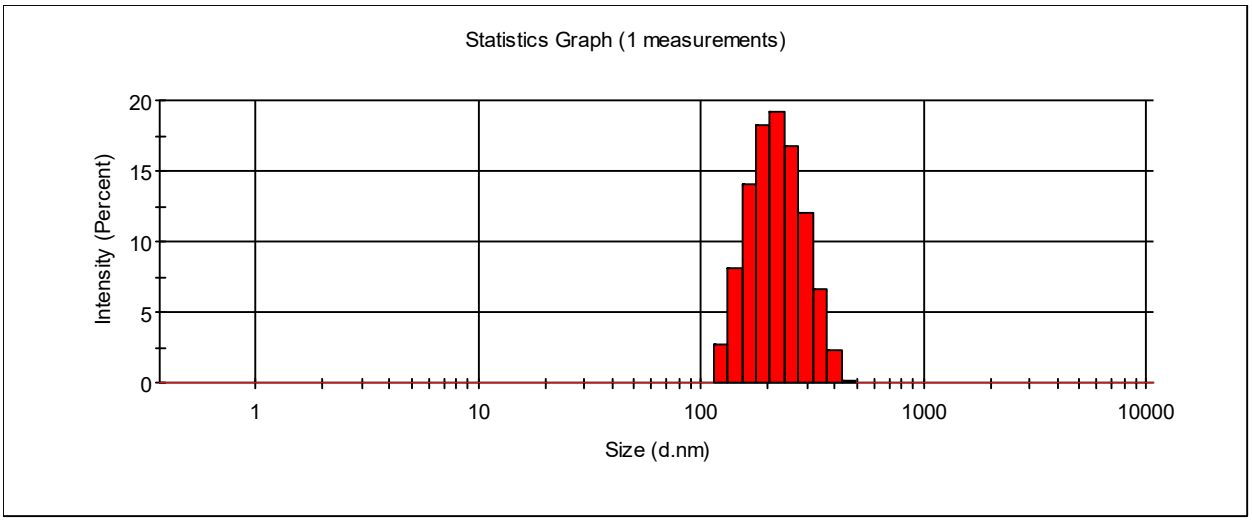

Fig. S5 (b). DLS data of **HL** (25 μM) at f_w = 50%

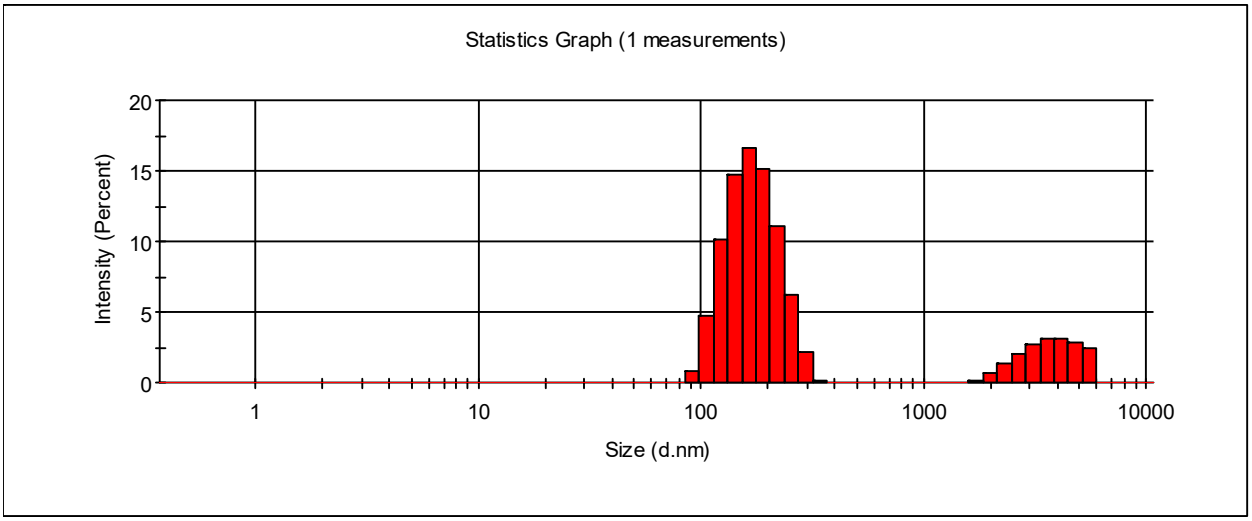

Fig. S5 (c). DLS data of **HL** (25 μM) at f_w = 70%

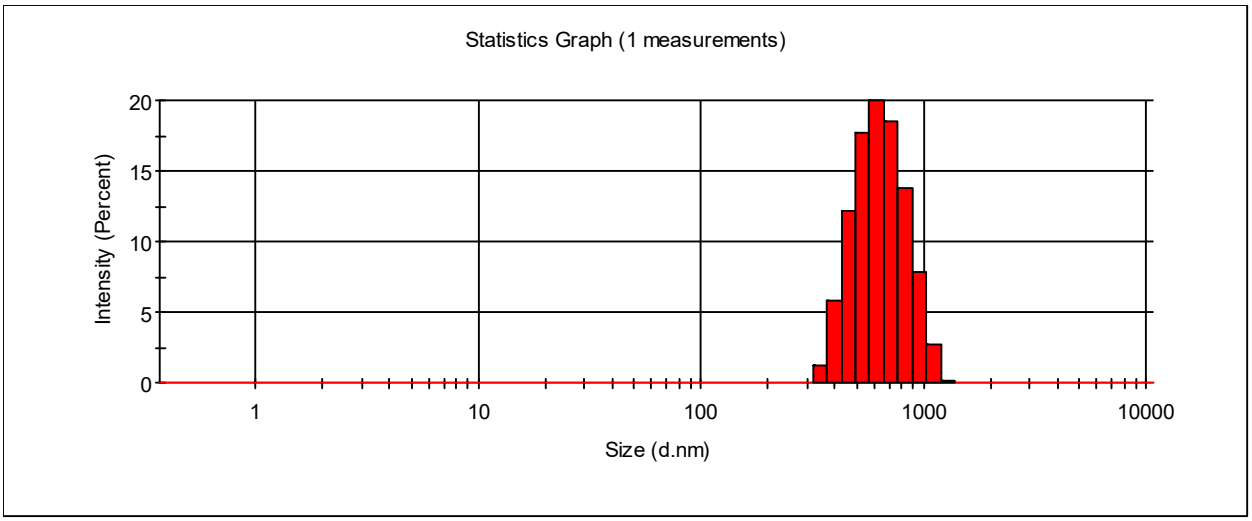

Fig. S5 (d). DLS data of **HL** (25 μM) at f_w = 95%

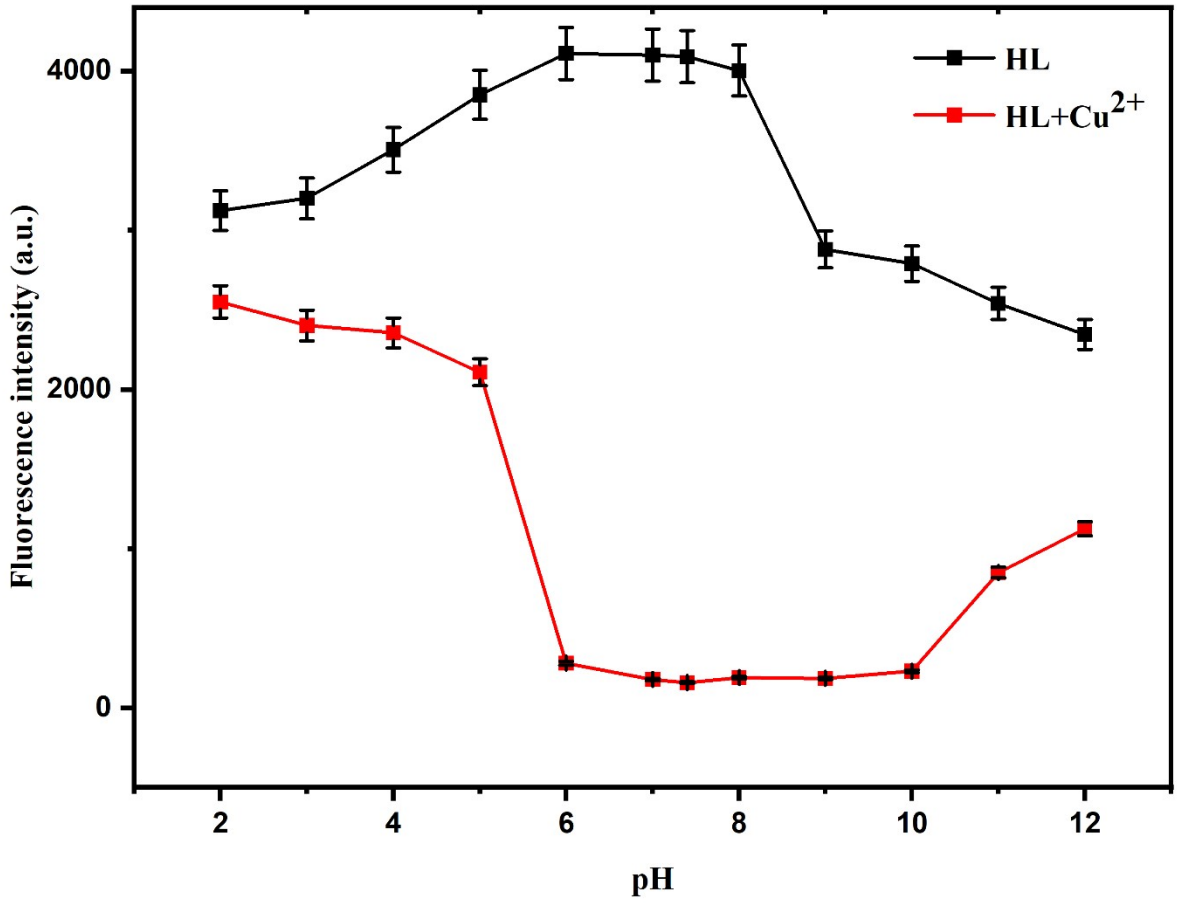

Fig. S6. Fluorescence spectra of **HL** with and without presence of copper in different pH

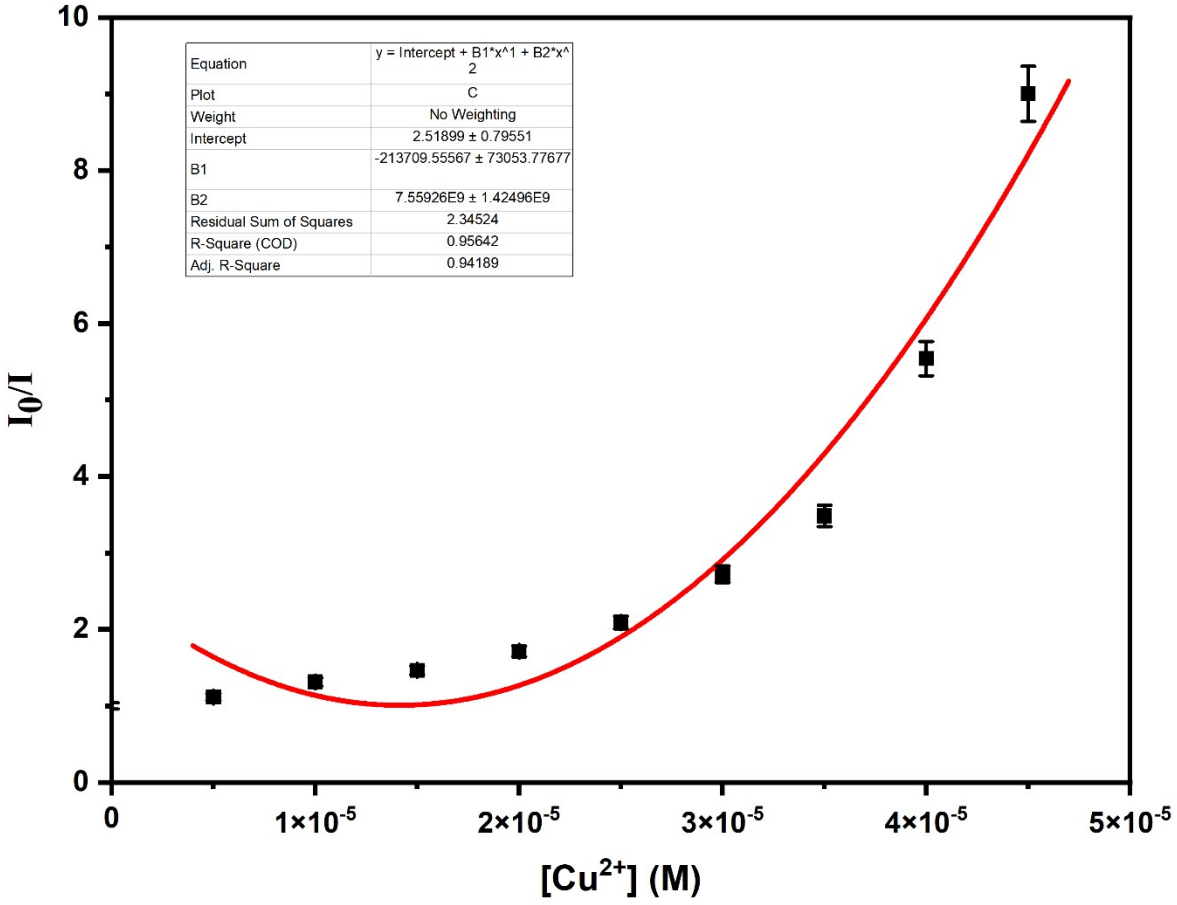

Fig. S7. Stern-volmer plot at high copper ion concentration

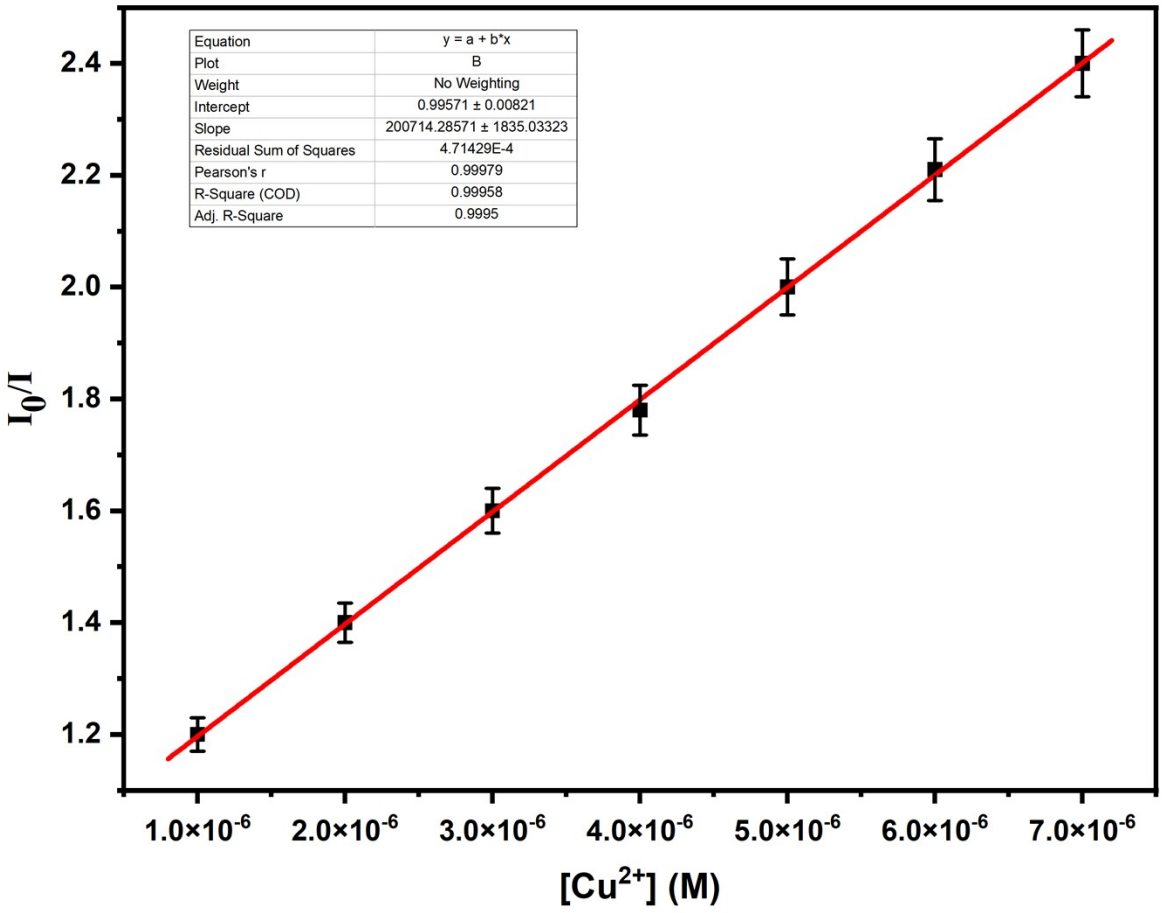

Fig. S8. Stern-volmer plot at low copper ion concentration

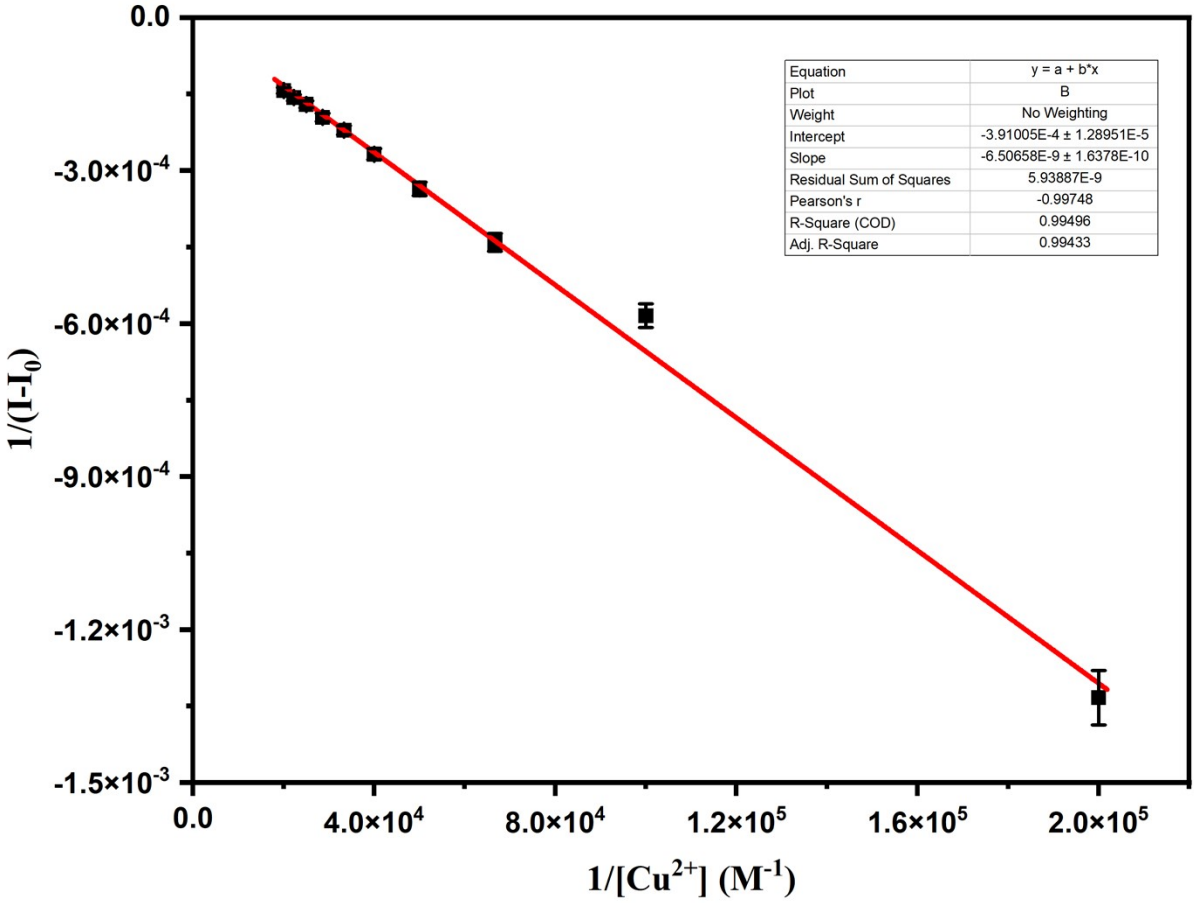

Fig. S9. BH-plot for binding contant determination

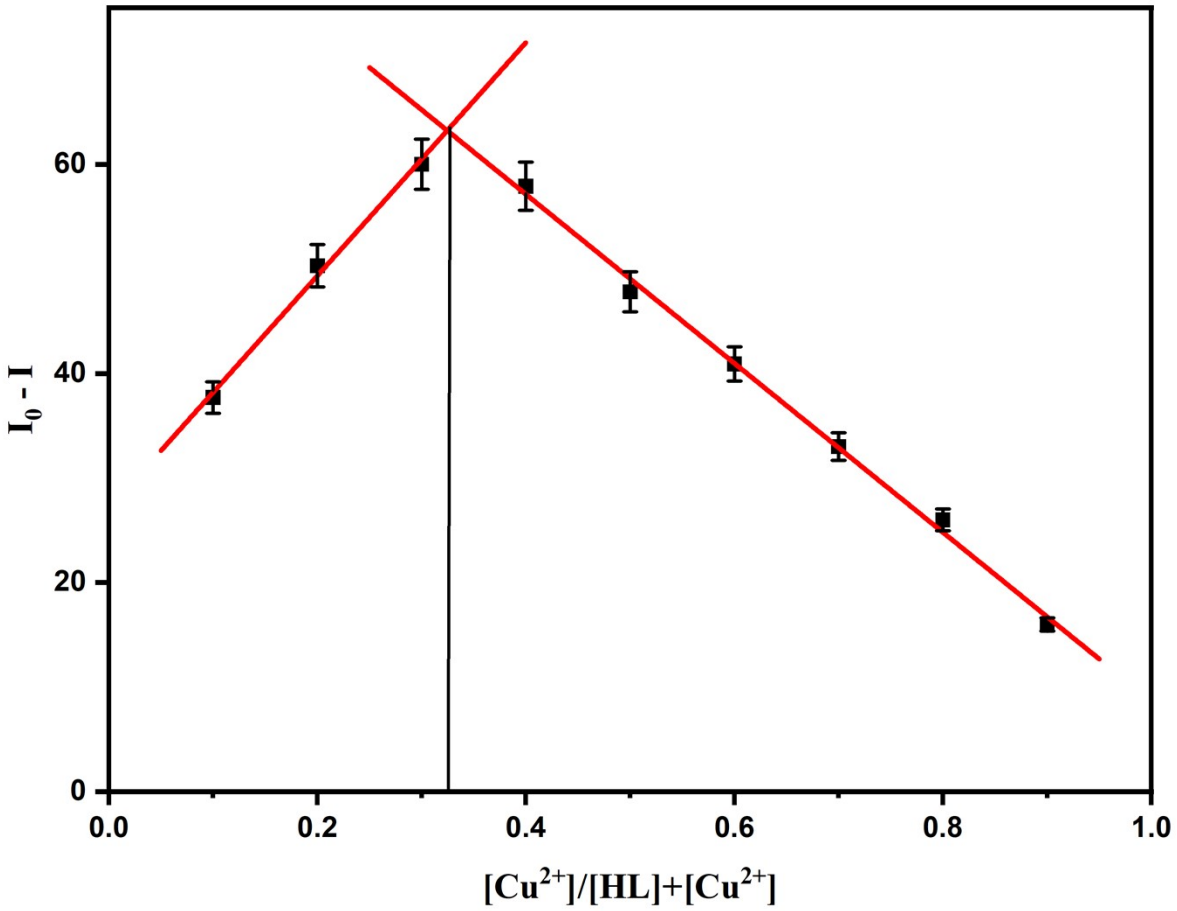

Fig. S10. Job's plot for binding stoichiometry determination

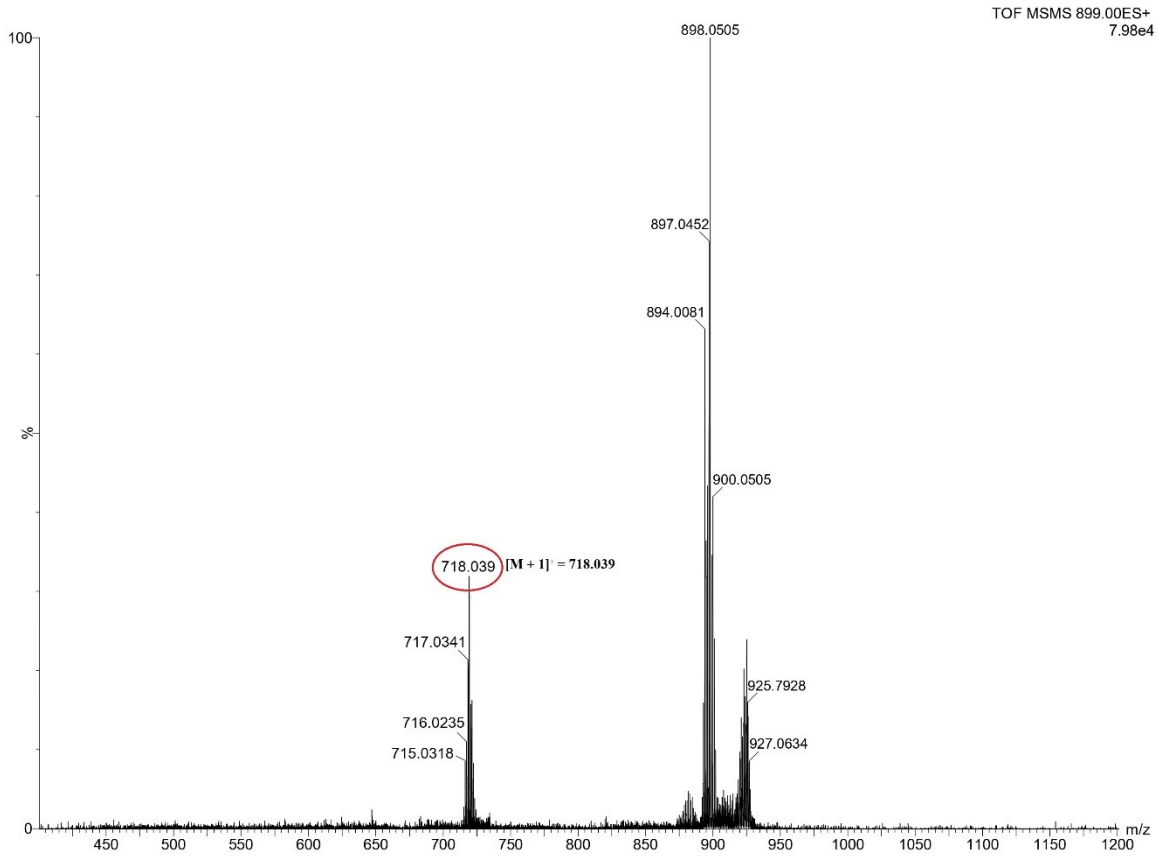

Fig. S11. ESI-MS spectra of **[HL+Cu^{2+}]** complex

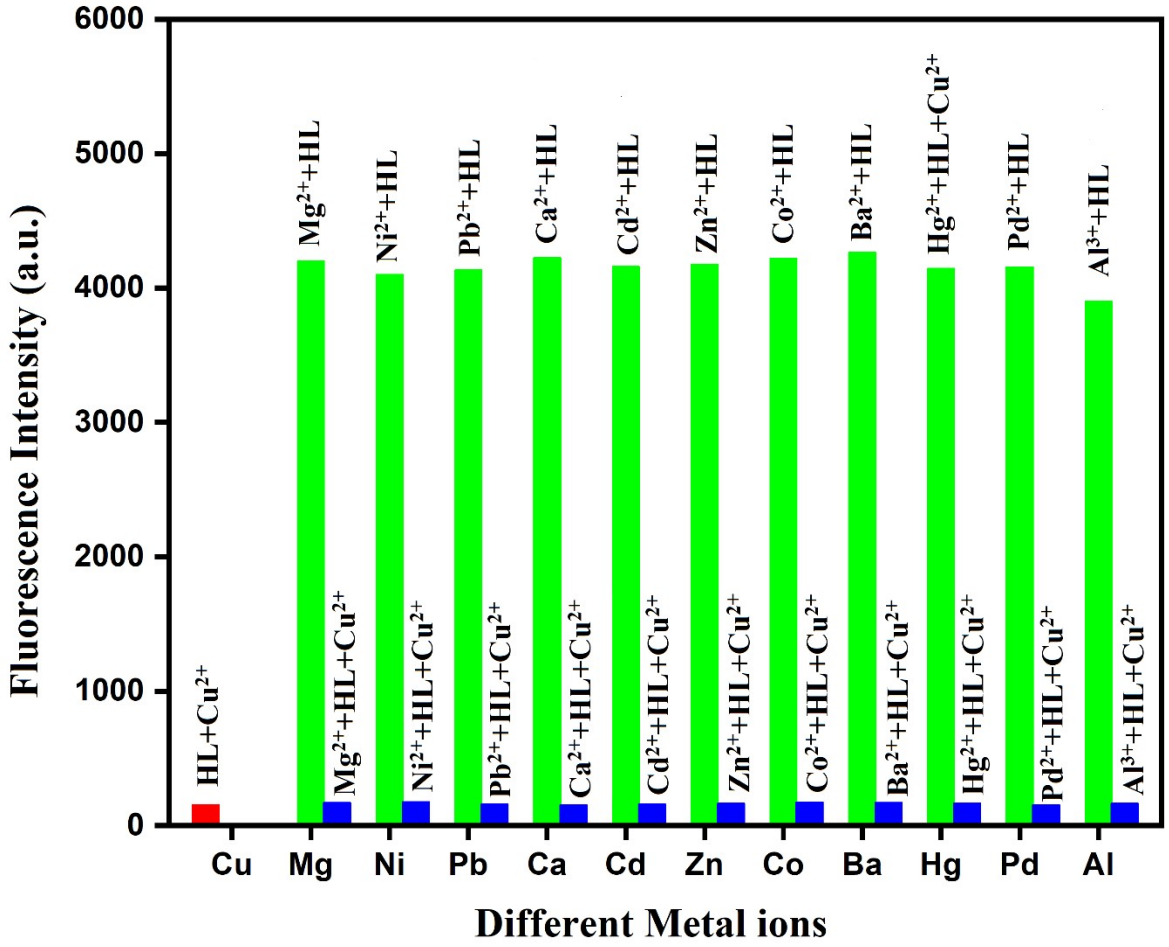

Fig. S12. Bar diagram illustrating interference study of **HL** (25 μM) with different metal ions (50 μM) in the solution of $f_w = 95\%$

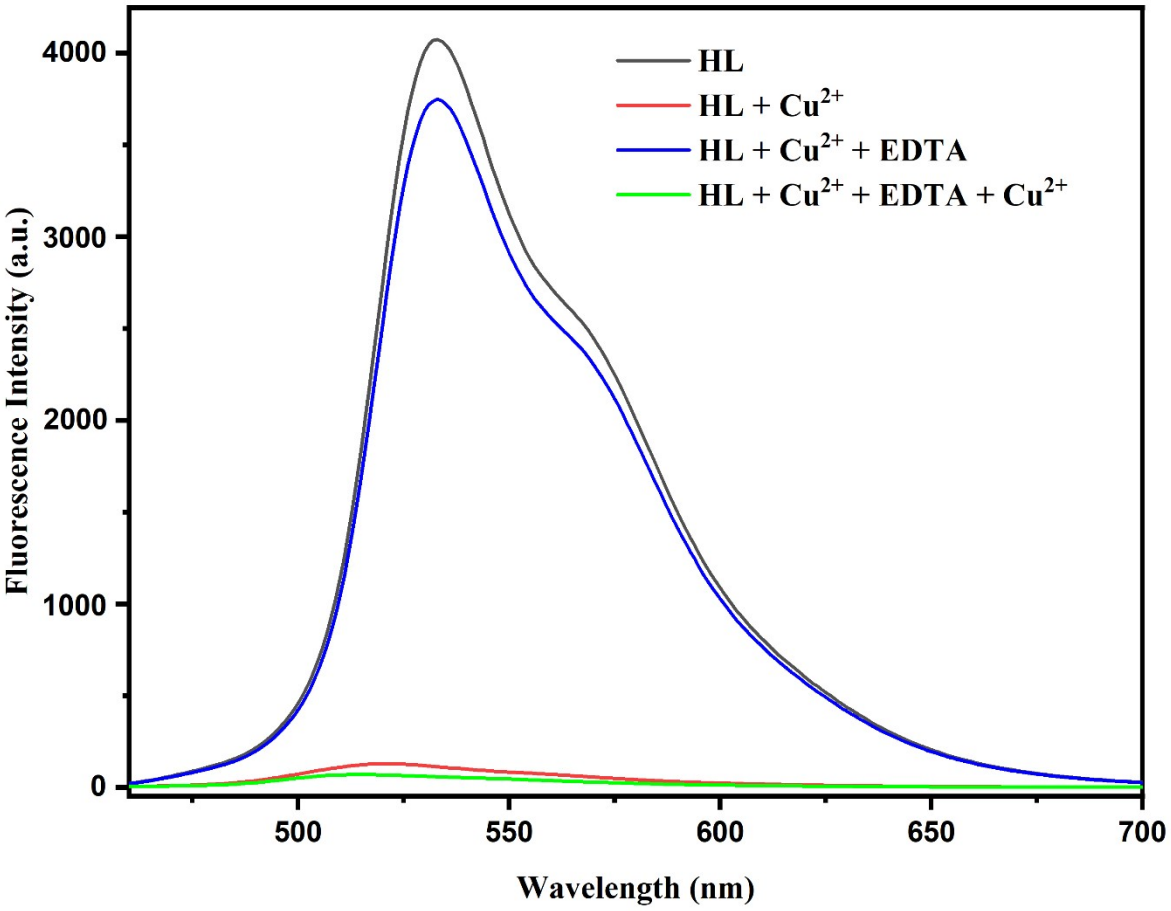

Fig. S13. Fluorescence spectra showing the reversible response of **HL** to Cu^{2+} (25 μM) after treatment with EDTA (25 μM).

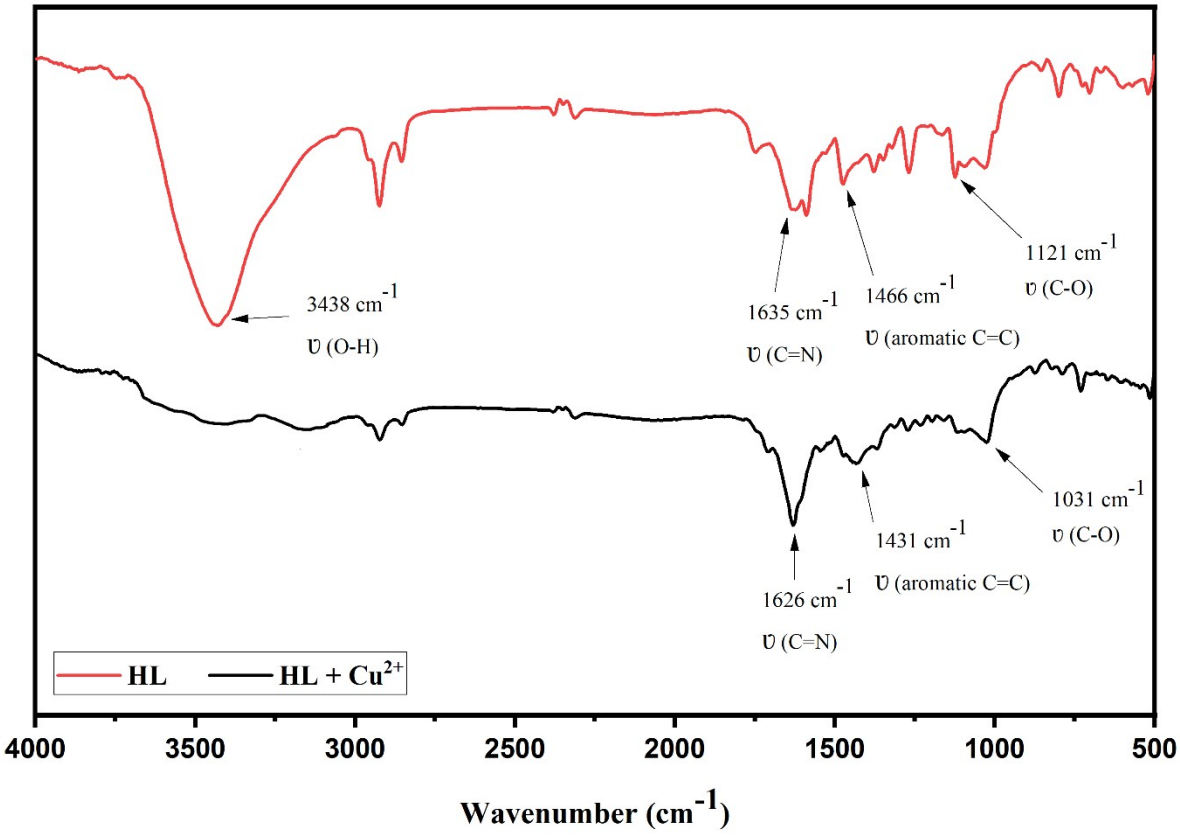

Fig. S14. FTIR comparison between **HL** and **HL+Cu^{2+}** complex

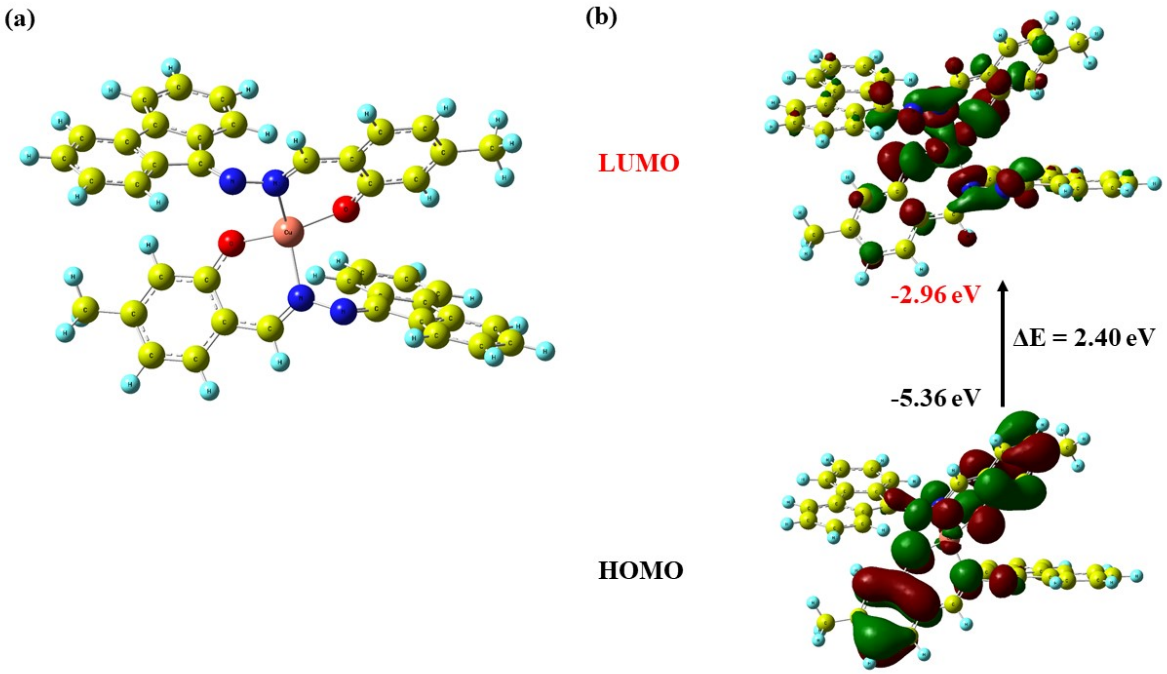

Fig. S15. (a) Optimized geometry of the **HL+Cu^{2+}** complex, and **(b)** HOMO and LUMO structures of the **HL+Cu^{2+}** complex.

Table S1. Crystal structure refinement parameters of **HL**

Identification code	**HL**
CCDC number	2483407
Empirical formula	$C_{21}H_{16}N_2O_2$
Formula weight	328.36
Temperature (K)	293(2)
Wavelength (Å)	0.71073
Crystal system	monoclinic
Space group	P_12_1/c_1
Unit cell dimensions	
a (Å)	10.2561(5)
b (Å)	7.5393(3)
c (Å)	21.0409(8)
α (deg)	90

β (deg)	98.471(4)
γ (deg)	90
Volume (Å^3)	1609.21(12)
Z	4
Calculated density (g/cm^3)	1.355
F (000)	688
Absorption coefficient (mm^{-1})	0.088
Crystal size (mm^3)	0.14×0.17×0.2
θ range (deg)	2.0060 to 26.6790
Limiting indices	$-13 \leq h \leq 13$, $-9 \leq k \leq 9$, $-27 \leq l \leq 26$
Reflections collected	3346
Independent reflections	2427
Data/restraints/parameters	3346/0/232
Goodness-of-fir on F^2	1.100
Final R indices [$I_o > 2\sigma(I_o)$]	0.0407, $wR_2 = 0.1090$
Final R indices (all data)	0.0599, $wR_2 = 0.1167$
Largest diff. Peak and hole (e·Å^{-3})	-0.127 and 0.157

Table S2. Bond lengths of **HL** from Crystallographic data

Atom 1	**Atom 2**	**Bond length (Å)**
O001	C00E	1.3584(16)
O001	C00P	1.4119(19)
O002	H002	0.8200
O002	C00C	1.3533(13)
N003	N004	1.3909(15)
N003	C00B	1.2957(15)
N004	C007	1.2930(15)
C005	C006	1.4098(17)

C005	C007	1.4910(17)
C005	C00H	1.3821(18)
C006	C009	1.4654(18)
C006	C00D	1.3840(17)
C007	C008	1.4737(18)
C008	C009	1.4008(17)
C008	C00G	1.3846(18)
C009	C00I	1.3819(18)
C00A	C00B	1.4272(18)
C00A	C00C	1.4005(18)
C00A	C00K	1.4099(17)
C00B	H00B	0.974(13)
C00C	C00F	1.3792(18)
C00D	H00D	0.9300
C00D	C00J	1.3754(19)
C00E	C00F	1.3829(17)
C00E	C00M	1.395(2)
C00F	H00F	0.9300
C00G	H00G	0.9300
C00G	C00O	1.3873(19)
C00H	H00H	0.9300
C00H	C00L	1.3925(18)
C00I	H00I	0.9300
C00I	C00N	1.384(2)
C00J	H00J	0.9300
C00J	C00L	1.3787(19)
C00K	H00K	0.9300
C00K	C00M	1.362(2)

C00L	H00L	0.9300
C00M	H00M	0.9300
C00N	H00N	0.9300
C00N	C00O	1.386(2)
C00O	H00O	0.9300
C00P	H00A	0.9600
C00P	H00C	0.9600
C00P	H00E	0.9600

Table S3. Bond angles of **HL** from Crystallographic data

Atoms	**Bond angles (°)**
C00E—O001—C00P	117.30(11)
C00C—O002—H002	109.500
C00B—N003—N004	111.96(11)
C007—N004—N003	116.23(10)
C006—C005—C007	107.26(11)
C00H—C005—C006	119.48(11)
C00H—C005—C007	133.25(12)
C005—C006—C009	109.40(11)
C00C—C00F—H00F	120.000
C00E—C00F—H00F	120.000
C008—C00G—H00G	120.700
C008—C00G—C00O	118.56(14)
C00O—C00G—H00G	120.700
C005—C00H—H00H	120.400
C005—C00H—C00L	119.19(13)
C00L—C00H—H00H	120.400

C009—C00I—H00I	120.800
C009—C00I—C00N	118.40(13)
C00N—C00I—H00I	120.800
C00D—C00J—H00J	119.600
C00D—C00J—C00L	120.84(12)
C00L—C00J—H00J	119.600
C00A—C00K—H00K	119.000
C00M—C00K—C00A	121.91(14)
C00M—C00K—H00K	119.000
C00H—C00L—H00L	119.600
C00J—C00L—C00H	120.71(14)
C00J—C00L—H00L	119.600
C00E—C00M—H00M	120.100
C00K—C00M—C00E	119.72(12)
C00K—C00M—H00M	120.100
C00I—C00N—H00N	119.500
C00I—C00N—C00O	121.08(14)
C00O—C00N—H00N	119.500
C00G—C00O—H00O	119.600
C00N—C00O—C00G	120.74(14)
C00N—C00O—H00O	119.600
O001—C00P—H00A	109.500
O001—C00P—H00C	109.500
O001—C00P—H00E	109.500
H00A—C00P—H00C	109.500
H00A—C00P—H00E	109.500
H00C—C00P—H00E	109.500
C00D—C006—C005	120.59(12)

Table S4. Torsion angles of **HL** from Crystallographic data

C00D—C006—C009	130.01(12)
N004—C007—C005	134.13(12)
N004—C007—C008	119.71(11)
C008—C007—C005	106.08(10)
C009—C008—C007	109.01(11)
C00G—C008—C007	130.56(12)
C00G—C008—C009	120.42(13)
C008—C009—C006	108.10(11)
C00I—C009—C006	131.10(12)
C00I—C009—C008	120.80(12)
C00C—C00A—C00B	122.07(11)
C00C—C00A—C00K	117.07(12)
C00K—C00A—C00B	120.84(12)
N003—C00B—C00A	122.79(13)
N003—C00B—H00B	117.9(7)
C00A—C00B—H00B	119.3(7)
O002—C00C—C00A	120.86(12)
O002—C00C—C00F	117.78(12)
C00F—C00C—C00A	121.36(11)
C006—C00D—H00D	120.500
C00J—C00D—C006	119.09(13)
C00J—C00D—H00D	120.500
O001—C00E—C00F	124.32(14)
O001—C00E—C00M	115.71(12)
C00F—C00E—C00M	119.97(13)
C00C—C00F—C00E	119.97(13)

Atoms	Torsion angles Bond angles (º)
O001—C00E—C00F—C00C	179.38(11)
O001—C00E—C00M—C00K	-179.23(11)
O002—C00C—C00F—C00E	-179.28(11)
N003—N004—C007—C005	0.76(19)
N003—N004—C007—C008	-175.54(9)
N004—N003—C00B—C00A	-179.45(10)
N004—C007—C008—C009	173.88(10)
N004—C007—C008—C00G	-4.6(2)
C005—C006—C009—C008	1.06(13)
C005—C006—C009—C00I	-178.51(12)
C005—C006—C00D—C00J	2.72(17)
C005—C007—C008—C009	-3.36(12)
C005—C007—C008—C00G	178.14(12)
C005—C00H—C00L—C00J	0.9(2)
C006—C005—C007—N004	-172.71(12)
C006—C005—C007—C008	3.95(12)
C006—C005—C00H—C00L	1.77(18)
C006—C009—C00I—C00N	179.32(12)
C006—C00D—C00J—C00L	-0.06(19)
C007—C005—C006—C009	-3.13(12)
C007—C005—C006—C00D	177.08(10)
C007—C005—C00H—C00L	-179.12(12)
C007—C008—C009—C006	1.51(13)
C007—C008—C009—C00I	-178.87(10)
C007—C008—C00G—C00O	179.25(12)
C008—C009—C00I—C00N	-0.20(18)
C008—C00G—C00O—C00N	-1.22(19)
C009—C006—C00D—C00J	-177.02(12)
C009—C008—C00G—C00O	0.89(18)
C009—C00I—C00N—C00O	-0.14(19)

C00A—C00C—C00F—C00E	0.0(2)
C00A—C00K—C00M—C00E	-0.4(2)
C00B—N003—N004—C007	-179.7(1)
C00B—C00A—C00C—O002	1.16(19)
C00B—C00A—C00C—C00F	-178.14(11)
C00B—C00A—C00K—C00M	178.32(12)
C00C—C00A—C00B—N003	-2.49(19)
C00C—C00A—C00K—C00M	-0.15(19)
C00D—C006—C009—C008	-179.18(12)
C00D—C006—C009—C00I	1.3(2)
C00D—C00J—C00L—C00H	-1.8(2)
C00F—C00E—C00M—C00K	0.71(19)
C00G—C008—C009—C006	-179.81(11)
C00G—C008—C009—C00I	-0.19(17)
C00H—C005—C006—C009	176.19(10)
C00H—C005—C006—C00D	-3.60(17)
C00H—C005—C007—N004	8.1(2)
C00H—C005—C007—C008	-175.24(13)
C00I—C00N—C00O—C00G	0.9(2)
C00K—C00A—C00B—N003	179.11(11)
C00K—C00A—C00C—O002	179.61(11)
C00K—C00A—C00C—C00F	0.31(18)
C00M—C00E—C00F—C00C	-0.56(19)
C00P—O001—C00E—C00F	-5.16(19)
C00P—O001—C00E—C00M	174.78(11)

Table S5. Photophysical properties of probe **HL** (50 μM) in different solvents.

Solvents	$\lambda_{abs\ (nm)}$[a]	ϵ (10^4 M^{-1} cm^{-1})	$\lambda_{em\ (nm)}$[b]	Stokes Shift (nm/cm^{-1})[c]	%Quantum Yield[d]
DMSO	350	3.2	550	200/ 50000	26.19
DMF	345	1.5	548	203/ 49261.1	32.45
ACN	330	1.9	516	186/ 53763.44	34.50
DCM	330	1.5	513	183/ 54644.8	30.11
THF	329	1.8	513	184/ 54347.82	22.45
$CHCl_3$	329	1.7	512	183/ 54644.8	27.89
Toluene	329	1.9	509	180/ 55555.56	24.55
Hexane	325	1.9	509	184/ 54347.82	24.68

[a] The absorption maximum in nm.

[b] The emission maximum in nm.

[c] Stokes shift calculated from absorption maximum to emission maximum.

[d] Fluorescence quantum yield.

Table S6. The average particle size of **HL** in different water fractions.

Average particle size in different water fractions (nm)			
f_w **= 30%**	f_w **= 50%**	f_w **= 70%**	f_w **= 95%**
145.36	204.05	222.78	547.21

Table S7. A comparison of previously published sensors based on detection of Cu^{2+} ions.

Sl no	Structure of Chemosensor	Emission wave length (nm)	LOD values (M)	Type of Fluorescence	Ref.
1	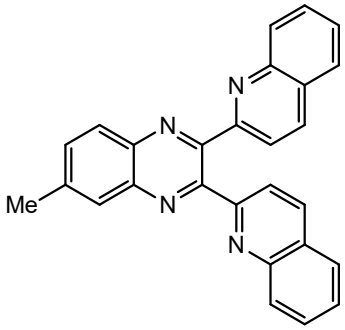	500	0.39×10^{-6}	Colorimetric	[13]
2	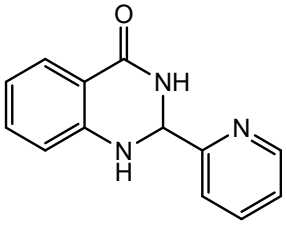	560	1.01×10^{-8}	Turn-off fluorescence	[14]

3	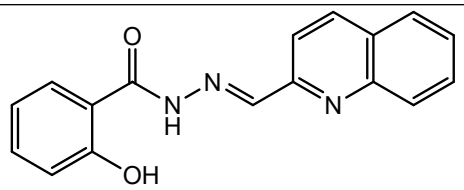	468	8.68×10^{-6}	On-off fluorescence	[15]
4	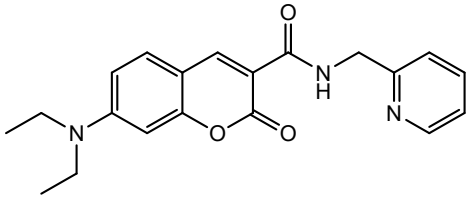	460	5×10^{-7}	Turn-off fluorescence	[16]
5	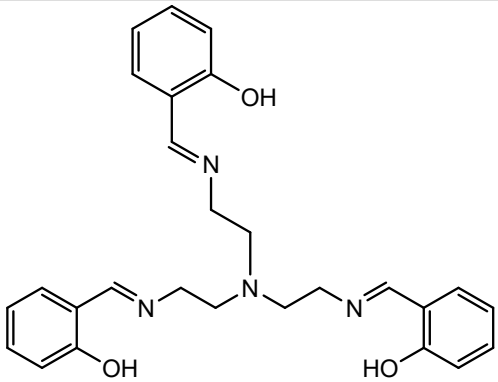	463	1.5×10^{-6}	Colorimetric	[17]
6	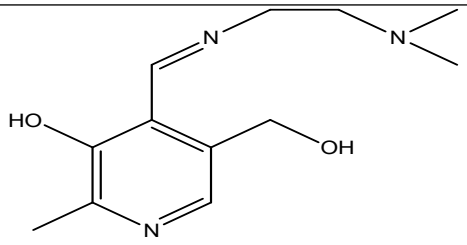	500	10×10^{-6}	Turn-on fluorescence	[18]
7	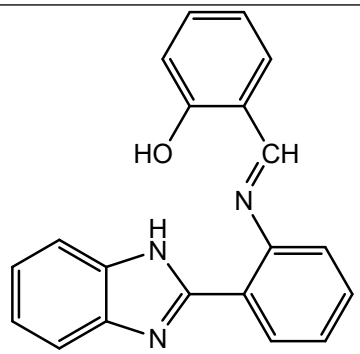	437	7.1×10^{-6}	Turn-off fluorescence	[19]

8	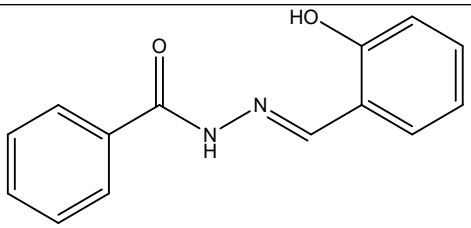	490	5.6×10^{-6}	Turn-off fluorescence	[20]
9	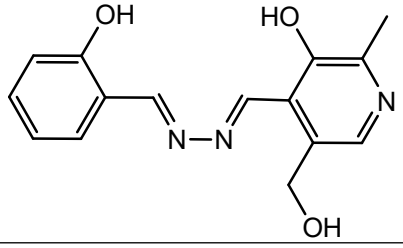	570	1.75×10^{-6}	Turn-off fluorescence	[21]
10	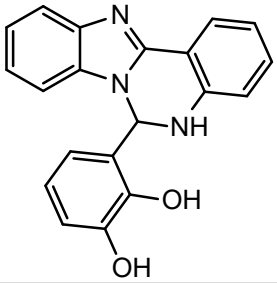	434	2.84×10^{-6}	On-off fluorescence	[22]
11	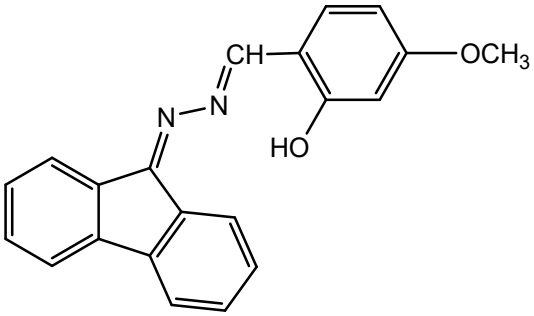	548	23.4×10^{-9}	Turn-off fluorescence	This work

Table S8. Real water and biological samples analysis by **HL** for copper ions.

Sources	**Test**	**Spiked (equivalent)**	**Found (equivalent)**	**Recovery Percentage (%)**	**R.S.D (n-3)**
Tap	T-1	0	-	-	-
	T-2	0.02	0.0194 ± 0.00056	97	0.137
Lake	T-3	0	-	-	-
	T-4	0.02	0.0189 ± 0.00045	94.5	0.269

River	T-5	0	-	-	-
	T-6	0.02	0.0202 ± 0.00011	101	1.063
Urine	T-7	0	-	-	-
	T-8	0.02	0.0179 ± 0.00081	89.5	0.607

References:

[1] A. Jain, P. Saraswat, S. De, H. Roy, B. Nath, S.S. Ghosh, P. Barman, Position-induced differential aggregation behavior with red-shifted emission: A case study of the promising copper ion sensor skeleton-based regio-isomers, J. Photochem. Photobiol. A Chem. 458 (2025) 115931.

[2] A. Schiafer, H. Horn, R. Ahlrichs, Fully optimized contracted Gaussian basis sets for atoms Li to Kr, J. Chem. Phys 97 (1992) 2571.

[3] A.D. Becke, Density-functional thermochemistry. III. The role of exact exchange, J. Chem. Phys. 98 (1993) 5648–5652.

[4] C.W. Bauschlicher Jr, H. Partridge, A modification of the Gaussian-2 approach using density functional theory, J. Chem. Phys. 103 (1995) 1788–1791.

[5] M.J. Snare, F.E. Treloar, K.P. Ghiggino, P.J. Thistlethwaite, The photophysics of rhodamine B, J. Photochem. 18 (1982) 335–346.

[6] M. Arshad, A. Paul, A. Joseph, Nanoscale detection of copper using an aggregation induced emission enhancement fluorescent sensor derived from hydroxy naphthaldehyde and benzyloxy benzaldehyde, J. Photochem. Photobiol. A Chem. 444 (2023) 114983.

[7] X.-J. Yan, Z.-G. Wang, Y. Wang, Y.-Y. Huang, H.-B. Liu, C.-Z. Xie, Q.-Z. Li, J.-Y. Xu, A dual-functional fluorescent probe for sequential determination of Cu2+/S2− and its applications in biological systems, Spectrochim. Acta Part A Mol. Biomol. Spectrosc. 243 (2020) 118797.

[8] J.R. Lakowicz, Instrumentation for fluorescence spectroscopy, in: Princ. Fluoresc. Spectrosc., Springer, 1999: pp. 25–61.

[9] S. Gurusamy, K. Krishnaveni, M. Sankarganesh, R.N. Asha, A. Mathavan, Synthesis, characterization, DNA interaction, BSA/HSA binding activities of VO (IV), Cu (II) and Zn (II) Schiff base complexes and its molecular docking with biomolecules, J. Mol. Liq. 345 (2022) 117045.

[10] S.O. Bahaffi, A.A.A. Aziz, M.M. El-Naggar, Synthesis, spectral characterization, DNA binding ability and antibacterial screening of copper (II) complexes of symmetrical

NOON tetradentate Schiff bases bearing different bridges, J. Mol. Struct. 1020 (2012) 188–196.

[11] B. Kumar, J. Devi, Chetna, B. Taxak, Insights into antimalarial and anti-tuberculosis activities of Schiff base transition metal complexes: molecular docking and ADMET profiling approaches, Res. Chem. Intermed. 51 (2025) 411–431.

[12] S. Sharma, A. Sharma, U. Gupta, Molecular Docking studies on the Anti-fungal activity of Allium sativum (Garlic) against Mucormycosis (black fungus) by BIOVIA discovery studio visualizer 21.1. 0.0, (2021).

[13] S.R. Alizadeh, P. Biparva, M.A. Ebrahimzadeh, A novel quinoxaline-based multifunctional probe: Sensitive and selective naked-eye detection of Fe3+ and fluorescent sensing of Cu2+ and its application, Arab. J. Chem. 17 (2024) 105724.

[14] P.N. Borase, P.B. Thale, G.S. Shankarling, Dihydroquinazolinone based “turn-off” fluorescence sensor for detection of Cu2+ ions, Dye. Pigment. 134 (2016) 276–284.

[15] C. Gao, X. Liu, X. Jin, J. Wu, Y. Xie, W. Liu, X. Yao, Y. Tang, A retrievable and highly selective fluorescent sensor for detecting copper and sulfide, Sensors Actuators B Chem. 185 (2013) 125–131.

[16] H.S. Jung, P.S. Kwon, J.W. Lee, J. Il Kim, C.S. Hong, J.W. Kim, S. Yan, J.Y. Lee, J.H. Lee, T. Joo, Coumarin-derived Cu2+-selective fluorescence sensor: synthesis, mechanisms, and applications in living cells, J. Am. Chem. Soc. 131 (2009) 2008–2012.

[17] K.B. Kim, H. Kim, E.J. Song, S. Kim, I. Noh, C. Kim, A cap-type Schiff base acting as a fluorescence sensor for zinc (II) and a colorimetric sensor for iron (II), copper (II), and zinc (II) in aqueous media, Dalt. Trans. 42 (2013) 16569–16577.

[18] S. Mandal, S.K. Mandal, A.R. Khuda-Bukhsh, S. Goswami, Pyridoxal based fluorescent chemosensor for detection of copper (II) in solution with moderate selectivity and live cell imaging, J. Fluoresc. 25 (2015) 1437–1447.

[19] W. Cao, X.-J. Zheng, D.-C. Fang, L.-P. Jin, Metal ion-assisted ring-opening of a quinazoline-based chemosensor: detection of copper (II) in aqueous media, Dalt. Trans. 44 (2015) 5191–5196.

[20] E. Espada-Bellido, M.D. Galindo-Riaño, M. García-Vargas, R. Narayanaswamy, Selective chemosensor for copper ions based on fluorescence quenching of a schiff-base fluorophore, Appl. Spectrosc. 64 (2010) 727–732.

[21] M. Umare, D.A. Patel, V. Bhardwaj, A.K. Sk, S.K. Sahoo, Pyridoxal Derived AIEgen for fluorescence turn-off sensing of Cu2+ and Fe2+ ions and fluorescence imaging of latent fingerprints, J. Fluoresc. 33 (2023) 601–611.

[22] D. Wang, J.-Q. Zheng, X.-J. Zheng, D.-C. Fang, D.-Q. Yuan, L.-P. Jin, A fluorescent chemosensor for the sequential detection of copper (II) and histidine and its biological applications, Sensors Actuators B Chem. 228 (2016) 387–394.